PNAS RESEARCH ARTICLE | ENVIRONMENTAL SCIENCES

Pan-European atmospheric lead pollution, enhanced blood lead levels, and cognitive decline from Roman-era mining and smelting

Joseph R. McConnell[a,1], Nathan J. Chellman[a], Andreas Plach[b], Sophia M. Wensman[a], Gill Plunkett[c], Andreas Stohl[b], Nicole-Kristine Smith[a,d], Bo Møllesøe Vinther[e], Dorthe Dahl-Jensen[e,f], Jørgen Peder Steffensen[e], Diedrich Fritzsche[g], Sandra O. Camara-Brugger[h], Brandon T. McDonald[a,i], and Andrew I. Wilson[j,k]

Affiliations are included on p. 6.

Edited by B. Turner, Arizona State University, Tempe, AZ; received September 25, 2024; accepted December 2, 2024

Ancient texts and archaeological evidence indicate substantial lead exposure during antiquity that potentially impacted human health. Although lead exposure routes were many and included the use of glazed tablewares, paints, cosmetics, and even intentional ingestion, the most significant for the nonelite, rural majority of the population may have been through background air pollution from mining and smelting of silver and lead ores that underpinned the Roman economy. Here, we determined potential health effects of this air pollution using Arctic ice core measurements of Roman-era lead pollution, atmospheric modeling, and modern epidemiology-based relationships between air concentrations, blood lead levels (BLLs), and cognitive decline. Findings suggest air lead concentrations exceeded 150 ng/m^3 near metallurgical emission sources, with average enhancements of >1.0 ng/m^3 over Europe during the Pax Romana apogee of the Roman Empire. The result was blood lead enhancements in young children of about 2.4 μg/dl above an estimated Neolithic background of 1.0 μg/dl, leading to widespread cognitive decline including a 2.5-to-3 point reduction in intelligence quotient throughout the Roman Empire.

lead pollution | lead poisoning | roman antiquity | human health | intelligence quotient

Significance

The detrimental effects of modern lead exposure on human health are widely recognized. Evidence from the Roman era indicates substantial lead exposure that potentially impacted human health more than 2,000 y ago. The most significant exposure for the rural, nonelite population may have been to background air pollution from silver mining and smelting that underpinned the Roman economy. Using detailed records of Roman-era lead pollution measured in Arctic ice cores and atmospheric modeling, we show that lead emissions from these activities elevated air concentrations throughout Europe. Based on modern epidemiological studies, this air pollution enhanced childhood blood lead levels (BLLs) by about 2.4 μg/dl leading to widespread cognitive decline including an estimated 2.5-to-3 point reduction in intelligence quotient.

The detrimental effects of lead exposure on human and ecosystem health during recent decades are widely recognized (1–3). With no known benefit for metabolism, essentially any level of lead exposure is thought to be damaging to human health, with infants and children particularly vulnerable (4–6). In 2021, the U.S. Centers for Disease Control and Prevention (CDC) lowered the reference blood lead level (BLL) for intervention in children from 5 μg/dl to 3.5 μg/dl, while noting that no BLL above zero is free of risk. Although higher levels of lead exposure have been linked to wide-ranging ailments in adults including infertility, anemia, nerve disorders and memory loss (7), health impacts at exposure levels much lower than in occupational settings include reduced renal function, lowered cognition, cardiovascular disease, cancer (8), and infertility (9). In children, low-level exposure has been linked to reduced intelligence quotient (IQ), concentration, and academic abilities (4, 10, 11). Negative health outcomes from childhood lead exposure are nonlinear, with proportionally greater impacts at very low (<5 μg/dl) concentrations (10–12). Even relatively limited exposure in early childhood during modern times has been linked to negative outcomes years or decades later such as reduced IQ and lifetime earnings (13).

Widespread exposure to atmospheric lead during the past 150 y resulted largely from coal, residual oil, and other fossil fuel burning, especially the ubiquitous use of leaded gasoline starting in the 1920s (14). Significant exposure to atmospheric lead pollution and potential human health effects, however, began thousands of years earlier as a result of early mining and metallurgy (15–20) documented in ancient texts such as Pliny the Elder's Natural History written in the 1st century CE (21) and evidenced by high lead concentrations in Roman-era skeletal (22) and dental remains (23). Fallout from atmospheric lead emissions during recent millennia is found in European peat and lake-sediment cores (24–26) and in Arctic and Alpine ice cores (17, 18, 27, 28). Exploiting the precise dating of the subannually resolved Arctic ice-core records, variations in lead pollution during antiquity have been linked to specific historical events such as the discovery, exploitation, and exhaustion of new mining regions in Iberia and Britain, and periods of social unrest such as the 1st century BCE crisis of the Roman Republic that immediately preceded the rise of the Roman Empire. Especially pronounced declines in lead pollution coincided with well-documented plague outbreaks such as the Antonine Plague (165 to 180 s CE) that severely affected the ancient world, with coeval reductions in the silver content of

The authors declare no competing interest.

This article is a PNAS Direct Submission.

[1]To whom correspondence may be addressed. Email: Joe.McConnell@dri.edu.

This article contains supporting information online at https://www.pnas.org/lookup/suppl/doi:10.1073/pnas.2419630121/-/DCSupplemental.

Published January 6, 2025.

Roman coinage (Fig. 1) demonstrating direct linkages to the economy (16, 29).

Ice-core records show that Arctic lead pollution was up to 40-fold higher during the early 1970s industrial maximum than during Greek and Roman times (17). Sources of atmospheric emissions during the late 19th through early 21st centuries were widespread across Europe and North America (30), with many sources located within or close to the Arctic. Conversely, emissions during antiquity came largely from ore smelting at or near relatively few southern, western, and eastern European lead/silver mining regions located thousands of kilometers from the ice coring sites (31). While potential routes for human exposure included lead in water pipes, utensils and pottery, toys, ornaments, cosmetics, and even intentional ingestion during antiquity (32–34), all Europeans, their livestock, and agricultural fields were exposed for centuries to background atmospheric lead pollution resulting from the large-scale mining and processing of lead/silver ores that underpinned the Greek and Roman economies (35). This background lead pollution in air and soil may have been the most significant exposure route in rural, nonelite populations. Here, we simulated metallurgy-related increases in European lead air concentrations during the apogee of the Roman Empire called the Pax Romana using atmospheric emissions determined from well-dated ice-core records of Arctic lead pollution and atmospheric aerosol modeling. Relationships from modern epidemiological studies were used to estimate minimum BLL enhancements from this air pollution and to assess potential regional and society-wide health impacts with a focus on childhood exposure and cognitive decline.

Results & Discussion

Lead Pollution in the Arctic. Nonbackground lead (nbPb) fluxes measured in a wide array of three Arctic ice cores (*Material and Methods*) spanning the period from 500 BCE to 600 CE, and atmospheric modeling (*SI Appendix*, Fig. S1) were used to estimate European lead emissions during antiquity. Temporal variations

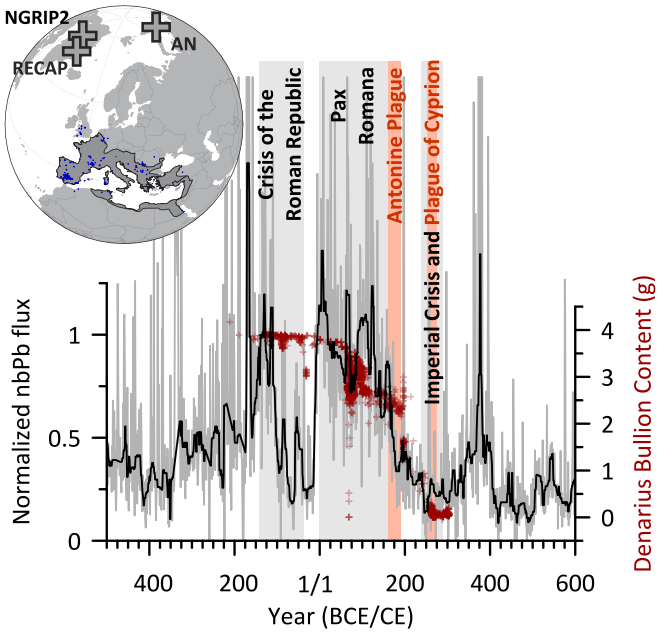

Fig. 1. Changes in Arctic lead pollution from 500 BCE to 600 CE and silver content in Roman coinage. Annual (gray) and 11-y median-filtered (black) average of normalized nonbackground lead (nbPb) fluxes from three Arctic ice cores (*SI Appendix*, Fig. S1), with major historical events and changes in silver bullion content in Roman coinage identified (29). The inset shows the outline of the extent of the Roman Empire in 14 CE and locations of ice cores (crosses) and Roman-era silver and lead mining sites (blue dots).

were similar at all the core sites to those reported previously for high-elevation coring sites on the Greenland ice sheet (16, 17, 36). Increases in nbPb deposition started during the Iron Age and reached an initial maximum in the late 2nd century BCE at the apex of the Roman Republic (Fig. 1). Deposition declined nearly to background levels during the 1st century BCE crisis of the Roman Republic and then sharply increased starting about 15 BCE soon after the start of the Roman Empire. The high lead fluxes that characterized the Pax Romana ended with the Antonine Plague from 165 to the 180s CE that severely affected the Roman Empire and the sustained high levels of nbPb flux during the Pax Romana were not exceeded until the High Middle Ages in the early 2nd millennium CE (17).

Roman-era Atmospheric Lead Emissions. The state-of-the-art atmospheric aerosol transport and deposition model FLEXPART [version 11 (37)] was used in backward and forward modes to estimate atmospheric concentrations and deposition fluxes throughout the Roman Empire from the lead deposition recorded in Arctic ice. First, we used backward FLEXPART simulations (*Materials and Methods*) (38) at 0.5° by 0.5° resolution to determine emission sensitivity fields for each core site (*SI Appendix*, Fig. S1). Second, the annual nbPb fluxes at the core sites and emission sensitivity fields were used to approximate annual atmospheric nbPb emissions (*SI Appendix*, Fig. S1) (15, 16, 39). Third, we used the three-core average emissions and forward FLEXPART simulations to estimate atmospheric nbPb concentrations and depositional fluxes across Europe during the Pax Romana, with forward simulations over Europe conducted at 0.25° by 0.25° resolution nested within global simulations at 0.5° by 0.5° resolution (Fig. 2). The ERA-5 reanalysis was used for all FLEXPART simulations (*Materials and Methods*). Simulation grid sizes over Europe were ~20 by ~28 km even using the higher-resolution reanalysis so air concentrations and fluxes immediately adjacent to emission sources probably were much higher. Typical simulated atmospheric transport times from European emission sources to the Arctic ice core sites are about 7 d, with more rapid and efficient transport in winter and spring when winds are more vigorous, and dryer atmospheric conditions result in less wet scavenging of aerosols during transport. The magnitude of emissions from individual Roman-era mining and metallurgy sites is unknown. Lacking more specific emission information, we conducted forward simulations for two endmember emission scenarios to assess a range of possible air concentrations.

Endmember emission scenario 1: Prior studies of lead isotopic ratios in the GRIP ice core from central Greenland (18) attributed emissions during the Roman period primarily to Rio Tinto which was a very large mining district in south-west Spain. Although somewhat unrealistic because other Roman-era mining and smelting sites are documented in the historical and archaeological records, to be consistent with the earlier study we simulated air concentrations assuming all of the observed lead pollution in the Arctic ice cores during the Pax Romana is attributed to emissions from Rio Tinto. Estimated lead emissions averaged ~4.2 kt/y, and forward FLEXPART modeling yielded European atmospheric lead concentrations ranging from 0.16 to 157 ng/m^3 with an average of 1.04 ng/m^3 over the northern (i.e., European) Roman Empire and 0.56 ng/m^3 over the southern (i.e., African) Empire (Fig. 2). As expected, concentrations were highest in the southern and central Iberian Peninsula near the Rio Tinto mining district. This emission rate of ~4.2 kt/y is similar to previous, less quantitative emission estimates based on historical and archaeological evidence of 4 kt/y (36) and our previous estimate for Rio Tinto emissions of 1.1 kt/y (16). The latter was based on a single ice-core record from a high-elevation

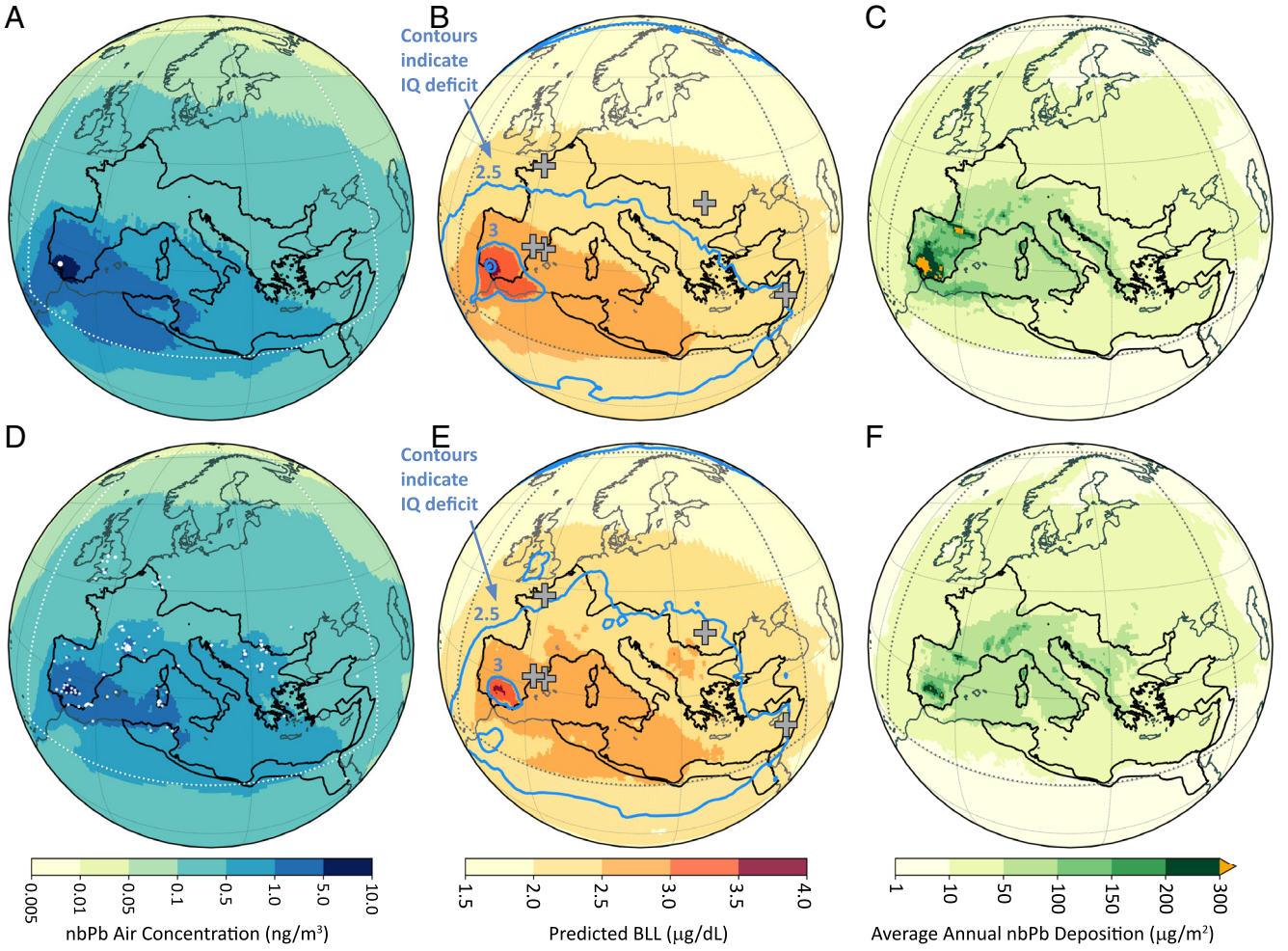

Fig. 2. Simulated annually averaged nonbackground lead (nbPb) concentrations in air, blood lead level (BLL) enhancements in young children with associated cognitive deficits, and average annual nbPb deposition during the Pax Romana. (*A*–*C*) Scenario 1 with emissions only from Rio Tinto (white dot). (*D*–*F*) Scenario 2 with emissions distributed equally among known Roman-era silver and lead mining sites (white dots). Blue contours in *B* and *E* show estimated IQ point changes resulting from enhanced BLLs. Crosses identify tooth enamel study sites. The dotted line shows the high-resolution FLEXPART model domain. The heavy black line delineates the extent of the Roman Empire in 14 CE.

site in northcentral Greenland and lower-resolution atmospheric simulations using an earlier version of FLEXPART and the CERA-20C reanalysis (40).

Endmember emission scenario 2: New measurements of lead isotopic ratios in the NGRIP2 ice core during and immediately following the Pax Romana (Fig. 3) suggest that emission sources were more varied. If emissions are distributed evenly among the known Roman-era mining and metallurgy sites (*Materials and Methods*), lower total atmospheric nbPb emissions of ~3.0 kt/y are implied. While maximum air concentrations over southern Iberia and northwestern Africa were substantially lower under the distributed scenario, simulated nbPb air concentrations over most of the northern Roman Empire were higher particularly over Gaul, Britannia, and the provinces east of the Adriatic. nbPb air concentrations ranged from 0.19 to 12.3 ng/m^3, averaging 0.79 and 0.49 ng/m^3 over the northern and southern Roman Empire, respectively (Fig. 2).

BLL Increases. To assess possible impacts on BLLs, we assumed that exposure to background air pollution from metallurgy added to preexisting baseline BLLs and used modern nonlinear relationships between air and blood concentrations (1) to estimate enhancements. Lead measurements in tooth enamel from Neolithic human remains (7) suggest a baseline BLL of about 1 μg/dl from inhalation of natural background particles in air and ingestion of lead-bearing food and water (*Materials and Methods*). For emissions scenario 1, BLL enhancements from nbPb air pollution ranged from 2.0 to 5.3 μg/dl in 1- to 5-y-old children (Fig. 2), resulting in average total BLLs of 3.4 μg/dl across both the northern and southern Roman Empire assuming a uniform population distribution (*Materials and Methods*). Similarly, estimated BLL enhancements ranged from 1.6 to 4.6 μg/dl in 6- to 11-y-old children, with averaged total BLLs of 3.9 and 2.9 μg/dl in the northern and southern Empire, respectively (*SI Appendix*, Fig. S2). For scenario 2, estimated enhancements ranged from 2.1 to 3.7 μg/dl in 1- to 5-y-old children in the northern and southern Roman Empire (Fig. 2), respectively, with average total BLLs of 3.5 and 3.3 μg/dl in the northern and southern Empire, respectively. Similarly estimated BLL enhancements ranged from 1.6 to 3.1 μg/dl in 6- to 11-y-old children, with average total values of 2.0 and 1.9 μg/dl in the northern and southern regions, respectively (*SI Appendix*, Fig. S2).

Measurements in tooth enamel from Roman-era skeletal remains indicate pervasive childhood lead exposure around the Roman Empire (23) that generally is consistent with these estimates. Lead is incorporated in tooth enamel during early childhood and concentrations even in ancient remains reflect childhood exposure. Unlike bones, lead in tooth enamel is not subject to diagenesis from the burial environment (23). Lead concentrations measured in tooth enamel from eleven Neolithic skeletal remains ranged from 0.03 to 0.27 μg/g, with an average of 0.11 μg/g and a geometric mean 0.09 μg/g (7). These levels of tooth enamel

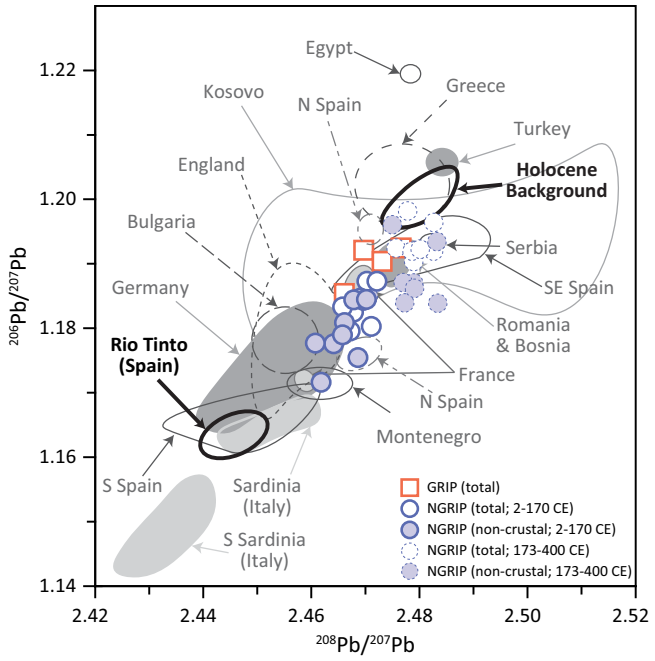

Fig. 3. Lead isotopic ratios in Greenland ice during and following the Pax Romana. Included are prior GRIP (18) and new NGRIP2 total and Holocene background-corrected measurements (*Materials and Methods*). Ellipses represent typical source compositions from Roman-era mining sites (*Materials and Methods*).

suggest (41) a baseline BLL of about 1.0 μg/dl. During the Roman period between the 1st and 4th centuries CE, tooth enamel measurements in 173 human remains from cemeteries (Fig. 2) around the Empire (23), including 59 fetal and young children (<2 y old) remains, generally were much higher. Implied BLLs (41) ranged from 0.3 to >1,800 μg/dl, with only seven (4%) individual BLLs below our minimum estimated Empire-wide averages of about 3.4 μg/dl enhanced by background air pollution exposure alone. Note that the burial year was not available so some of the individuals may have lived after the period of high atmospheric lead pollution during the Pax Romana and so received less exposure.

Cognitive Declines. We used modern epidemiological linkages between childhood BLLs and IQ (42) to assess possible cognitive declines associated with enhanced BLLs from air lead pollution. Focusing on 1- to 5-y-olds, these linkages suggest that enhanced BLLs under emission scenario 1 resulted in additional IQ deficits ranging from 2.3 to 4.3 points, with deficits of >4 IQ points in areas immediately surrounding Rio Tinto and between 2.5 and 3 IQ points throughout most of the Roman Empire south of ~45°N (Fig. 2). Under emission scenario 2, deficits were >3 IQ points in the mining regions concentrated in southern Iberia and between 2.5 and 3 IQ points across nearly all the Roman Empire including most of Britannia (Fig. 2). For perspective, the modern geometric mean BLL measured in 1- to 5-y-old US children was 15.2 μg/dl between 1976 and 1980 soon after the start of lead pollution mitigation efforts including the phasing out of leaded gasoline, declining to 0.8 μg/dl between 2011 and 2016 (43). These BLLs correspond to IQ deficits of 9.2 (±1.7 SD) and 1.9 (±0.4 SD), respectively.

Conclusions

Our findings, underpinned by Arctic ice-core records and atmospheric modeling, suggest that nbPb concentrations in ambient air were elevated sufficiently by emissions from silver and lead mining and metallurgy to cause neurological effects across the Roman Empire during the Pax Romana, including population-wide IQ reductions of 2.5 to 3 points in addition to what might be expected from Neolithic BLLs. Because they are based only on primary atmospheric emissions, we emphasize that the air concentrations and BLLs presented here probably are minimum estimates even in rural, nonelite populations with limited or no exposure to other sources of lead poisoning. Our results suggest that >500 kt of lead were released to the atmosphere during the nearly 175-y Pax Romana, with the bulk deposited over the Roman Empire (Fig. 2) undoubtedly contaminating surface soils with lead as observed from modern nonferrous smelters (44). Lead adsorbed onto larger dust particles would have been deposited closer to sources, further enriching local dust sources (*SI Appendix*, Fig. S3). Although difficult to quantify because lead accumulation in soils and so local dust concentrations depend on mobilization, which is controlled by soil pH, mineralogy, and other factors (45), these enriched soils very likely enhanced exposure especially in young children resulting in higher BLLs and even greater cognitive declines. Immune system impairment also has been linked to low-level lead exposure (46) so it is intriguing that the prolonged, destructive, and infectious Antonine Plague—the first great epidemic of the Roman Empire that killed an estimated 5 to 10 million people or roughly 10% of the population in cities and rural, nonelite communities alike (47)—immediately followed nearly two centuries of highly elevated atmospheric lead emissions from European mining and metallurgy (Fig. 1) that resulted in widespread lead exposure at levels never before experienced by a civilization.

Materials and Methods

Ice Core Records. Concentrations of lead and a range of other elements and chemical species were measured continuously in archived samples from three Arctic ice cores using the well-established DRI continuous ice core analytical system (48, 49). Included were the previously published Akademii Nauk record (80.5°N, 94.8°E) from Severnaya Zemlya in the Russia Arctic (17, 50) and North Greenland Ice Core Project (NGRIP2; 75.1°N, 43.3°W) record from northcentral Greenland (16), as well as the new RECAP record (71.3°N, 26.7°W) (51) from the Renland ice cap in east Greenland. This ice-core array spans 141.6° of longitude and 9.2° of latitude and so is representative of lead pollution deposition over a large fraction of the Arctic.

Following McConnell et al. (15), noncrustal lead (ncPb) concentrations were derived from measured total lead concentrations using simultaneous measurements of the rock-forming rare earth element cerium [after correction by 1.6 for underrecovery during the continuous measurement (52, 53)] and relative mean soil abundances for lead and cerium of 19 and 83 (54), respectively. As in prior studies based on spatial arrays of ice core aerosol records (15, 17, 39), annual average concentrations and fluxes were determined from the continuous measurements. Following (16, 17), nonbackground lead (nbPb) fluxes were determined from ncPb fluxes by subtracting an estimated constant volcanic flux from each record.

All three cores were dated by multiparameter annual layer counting constrained by fallout from explosive volcanism, with dates of the fallout based on the NGRIP2 ice core chronology (16). The NGRIP2 chronology is well within the uncertainties of the GICC21 (55) and NEEM-2011-S1 (56) timescales during antiquity. Evaluations against cosmogenic nuclide concentrations in the NGRIP2 ice core and well-dated tree-core samples (56, 57) suggest uncertainties in the ice core chronologies of ± 2 y during the 1st century BCE (16). Fallout of radiatively important sulfur from the massive Okmok II volcanic eruption and simulated cooling as a result coincided exactly with pronounced Northern Hemisphere cooling recorded in tree rings (58) suggesting no age uncertainty in the DRI_NGRIP2 chronology at that depth if the tree-ring chronology is assumed to be accurate. Tephra particles from the Okmok II eruption previously found in GISP2 ice dated to 43 BCE on the DRI_NGRIP2 age scale (58) also were found in 43 BCE in NGRIP2 and RECAP ice, thereby confirming the age synchronization between these cores and the tree-ring chronology (*SI Appendix*, Fig. S4).

Atmospheric Aerosol Deposition and Transport Modeling. Following previous ice core aerosol studies (15–17, 39), the state-of-the-art atmospheric aerosol transport and deposition model FLEXPART (59) was used in backward mode

to determine emission sensitivity fields (38) at all three core sites. Lacking the detailed meteorological fields necessary for such modeling during antiquity, we assumed as in prior studies (15–17, 39) that meteorological conditions driving atmospheric transport during ancient times were similar to the 20th century so backward FLEXPART [version 11 (37)] simulations were conducted for 10 y (1960 to 1969) using global ERA-5 reanalysis data [0.5° × 0.5° resolution, 137 vertical layers of which 41 are located below 5,000 m asl (60)].

As in past studies (16), we assumed that lead emitted from metallurgical processes in the gaseous phase quickly adsorbed onto ambient 1 μm dust particles and these small, relatively inert particles were transported to Greenland and deposited through both wet and dry deposition. To test sensitivity of the results to the assumed ambient aerosol type, however, we also performed separate calculations for mineral dust with a diameter of 5 μm, as well as sulfate and black carbon aerosols with assumed diameters of 0.4 μm.

With atmospheric lead emissions constrained by the ice core pollution records and backward FLEXPART simulations, we used forward FLEXPART simulations to estimate atmospheric lead concentrations and depositional fluxes across Europe. Forward simulations corresponding to the 1960 to 1969 decade were conducted with higher-resolution meteorological ERA-5 data over Europe (0.25° × 0.25° over the domain 30 to 72°N and 15 to 40°E) nested into the global 0.5° × 0.5° data, assuming constant emission rates for two different scenarios (Fig. 2): 1) emissions of 4.2 kt/y only from a single source located near Rio Tinto (37.4°N, 6.5°W) in southern Iberia, and 2) emissions of 3.0 Kt/y distributed equally among known antiquity-era European mining and smelting operations (Figs. 1 and 2) (16, 31). The latter estimates are slightly lower because the average emissions sensitivities for the distributed sites are higher than those for Rio Tinto alone. Model grid sizes for the high-resolution 0.25° × 0.25° forward simulations over Europe ranged from ~24 by ~28 km at 30°N to ~9 km by ~28 km at 72°N.

Lead Isotopic Ratios. Lead isotopic ratios were measured in NGRIP2 meltwater samples (*SI Appendix*, Table S1) routinely collected as part of the continuous ice core measurements (16). Reconstituted, acidified meltwater samples were analyzed following established methods (15, 27). Samples were introduced into an Element2 h-ICP-MS (Thermo) using an Apex IR inlet system fitted with a PFA MicroFlow nebulizer (Elemental Scientific) and N_2 was used as the additional gas. The low abundance of ^{204}Pb in the environment (1.4% of total lead) combined with low lead concentrations present in ice core meltwater samples (<1 ng g^{-1}) precluded precise determination of ^{204}Pb levels, so we only used ratios of the more abundant ^{206}Pb (24.1%), ^{207}Pb (22.1%), and ^{208}Pb (52.4%) isotopes.

All samples and standards were normalized to the bracketing standard (National Institute of Standards and Technologies (NIST) SRM 981 natural lead (isotopic) standard). Procedural blanks contributed an average of 0.02 ± 0.02% of the sample lead signal. Measured reference materials differed from published values (61) for BCR-2 Columbia River Basalt and AGV-1 Guano Valley Andesite, and (27) NIST 1643f Trace Elements in Water) by 0.16% for $^{206}Pb/^{207}Pb$ and 0.02% for $^{208}Pb/^{207}Pb$ (*SI Appendix*, Table S2). An in-house reference material Bulk-B composed of surface snow samples from central Greenland also was measured to assess repeatability and is thought to best reflect precision of meltwater from the NGRIP2 ice core (*SI Appendix*, Table S2).

A simple linear mixing model was used to calculate the noncrustal lead isotopic ratios.

$$X_S = f_c X_c + f_{nc} X_{nc},$$

$$f_c + f_{nc} = 1,$$

where the isotopic ratio of the measured sample (X_S) is determined by the isotopic ratios of the endmembers, defined as the crustal (X_c) and noncrustal (X_{nc}) isotopic composition multiplied by the fraction of lead each endmember contributes (f_c and f_{nc}, respectively). The fractions of crustal lead (f_c) and noncrustal lead (f_{nc}) were determined using the measured concentrations of lead and the rock-forming rare earth element cerium (Ce) [after correction by 1.6 for underrecovery during continuous measurements (52, 53)], as well as the relative mean soil abundances for lead and cerium of 19 and 83 (54), respectively. The previously established Holocene background lead isotopic ratios (1.201 ± 0.005 for $^{206}Pb/^{207}Pb$ and 2.482 ± 0.005 for $^{208}Pb/^{207}Pb$ (18) were used to represent the average crustal lead isotopic signature (X_c). Total and corrected lead isotopic ratios were compared to similar ratios from ores in regions mined during the Pax Romana (Fig. 3), including Spain (62–64), Germany (65, 66), Bulgaria (67), England (68, 69), Kosovo (70, 71), Egypt (72), Greece (73–76), Türkiye (74), Serbia (70), Romania (77), Bosnia (70, 78), France (79), Montenegro (70), and Italy (74). Total lead isotopic ratios also were compared to previously established ice core background lead isotopic ratios from the Holocene (18).

BBLs and Effects on Human Health. We used recently reported, nonlinear relationships between (1) ambient air and blood lead concentrations (1) for different age groups to estimate enhanced BLLs from the FLEXPART-simulated air concentrations, and (2) modern linkages between BLLs and IQ (10, 42) to assess likely levels of additional cognitive decline resulting from early childhood exposure to air pollution from mining and metallurgy during the Pax Romana. To estimate BLLs (μg/dl) enhancements from ambient air concentrations (1), we used a log-linear model BLL = exp[1.932(±0.181) + 0.140(±0.054) × ln(air concentration)] for 1- to 5-y-old children and BLL = exp[1.812(±0.279) + 0.154(±0.083) × ln(air concentration)] for 6- to 11-y-old children. To estimate IQ deficits from concurrent BLLs (42), we used a log-linear model with IQ deficit = −3.315(±0.6155) × ln(BLL + 1). For both models, reported uncertainties are 1 SD. Lacking information on the spatial distribution of the population around the empire, we assumed a uniform distribution to derive average BLL and IQ deficit enhancements.

Uncertainty Estimates. We estimate that the coefficient of variation on the average IQ deficits resulting from background atmospheric nbPb exposure to be about 0.9. While the error propagation included terms for atmospheric emissions and concentration, BLL, and IQ deficit, the largest terms were associated with (1) the FLEXPART-simulated emission sensitivity used to determine atmospheric nbPb emissions from Roman-era mining and metallurgy and (2) the calculation of estimated BLLs from air concentrations (1). FLEXPART simulations longer than 10 y would reduce uncertainties in the emission sensitivities. The estimated emissions were based on the magnitude of the aerosol deposition determined from the ice core measurements, and comparisons of replicate continuous measurements of parallel samples cut from the same ice core suggest that measurement uncertainties for lead and cerium are low (<10%) (80). The emission sensitivity, however, which depends on the precipitation input used by FLEXPART and the scavenging properties of the aerosol, may be subject to systematic model biases and these may be especially important when simulating long-range atmospheric transport (e.g., >4,000 km from mid-latitude emission sources to Arctic ice core sites). Comparisons of the four model tracers evaluated in FLEXPART suggest an uncertainty range of a factor of two or more in the overall magnitude of the atmospheric nbPb emissions; here we assumed a coefficient of variation of 0.67 (16, 39). Note also that while backward FLEXPART simulations of aerosol transport and deposition were conducted at a relatively high 0.5° × 0.5° spatial resolution, ice-core records represent deposition at a single location that may or may not be representative of the surrounding region. This is particularly the case for the magnitude of aerosol deposition which depends strongly on the amount and seasonal timing of net snow accumulation at a specific ice core site. To mitigate any site-specific biases, the atmospheric emissions used in the two emission scenarios and to assess health impacts were the result of averaging emission estimates from the three individual ice core sites.

Data, Materials, and Software Availability. Total and non-background annual lead deposition data in three Arctic ice cores, as well as the results of forward and backward FLEXPART simulations, are included in the supporting information online.

ACKNOWLEDGMENTS. This study on the health effects of lead emissions during antiquity was supported by NSF Grant 1925417 to J.R.M. Continuous chemical analyses of the RECAP and Akademii Nauk ice cores at DRI were funded by NSF Grants 1925417 and 1023672 to J.R.M., respectively. Analysis of archived NGRIP2 samples at DRI was supported by the John Fell Oxford University Press Research Fund and All Souls College, Oxford, as well as the Desert Research Institute. NGRIP2 lead isotopic measurements and interpretation were funded by NSF Grant 2138782 to S.M.W. Support for S.O.C.-B. was provided by Swiss NSF Grant P400P2_1999285. We gratefully acknowledge the students and staff of the DRI ultratrace ice core laboratory as well as the NGRIP, Akademii Nauk and RECAP field teams for their efforts to collect the ice cores. We also acknowledge the use of ECMWF's computing and archive facilities provided through a special project (spatvojt). The FLEXPART computational results presented here have been achieved in part using the Vienna Scientific Cluster (VSC).

Author affiliations: [a]Division of Hydrologic Sciences, Desert Research Institute, Reno, NV 89512; [b]Department of Meteorology and Geophysics, University of Vienna, Vienna 1090, Austria; [c]School of Natural and Built Environment, Queen's University Belfast, Belfast BT7 1NN, United Kingdom; [d]Environmental Health Sciences, Yale School of Public Health, New Haven, CT 06520; [e]Physics of Ice, Climate and Earth, Niels Bohr Institute, University of Copenhagen, Copenhagen DK 2200, Denmark; [f]Centre for Earth Observation Science, University of Manitoba, Winnipeg, MB R3T 2N2, Canada; [g]Polar Terrestrial Environmental Systems, Alfred-Wegener-Institut Helmholtz-Zentrum für Polar-und Meeresforschung, Potsdam 14473, Germany; [h]Department of Environmental Sciences, University of Basel, Basel 4056, Switzerland; [i]Department of Classical Studies, Tufts University, Medford, MA 02155; [j]Institute of Archaeology, University of Oxford, Oxford OX1 4PG, United Kingdom; and [k]Faculty of Classics, University of Oxford, Oxford OX1 3LU, United Kingdom

Author contributions: J.R.M. and A.S. designed research; J.R.M., N.J.C., A.P., S.M.W., G.P., B.M.V., D.D.-J., J.P.S., D.F., S.O.C.-B., and B.T.M. performed research; J.R.M., N.J.C., A.P., S.M.W., G.P., A.S., and N.-K.S. analyzed data; and J.R.M., N.J.C., A.P., S.M.W., G.P., A.S., and A.I.W. wrote the paper.

1. J. Richmond-Bryant *et al.*, The influence of declining air lead levels on blood lead–air lead slope factors in children. *Environ. Health Perspect.* **122**, 754–760 (2014).
2. J. A. Paulson, M. J. Brown, The CDC blood lead reference value for children: Time for a change. *Environ. Health* **18**, 16 (2019).
3. K. E. Giller, E. Witter, S. P. McGrath, Toxicity of heavy metals to microorganisms and microbial processes in agricultural soils: A review. *Soil Biol. Biochem.* **30**, 1389–1414 (1998).
4. B. P. Lanphear, Low-level toxicity of chemicals: No acceptable levels? *PLOS Biol.* **15**, e2003066 (2017).
5. D. C. Bellinger, Very low lead exposures and children's neurodevelopment. *Curr. Opin. Pediatr.* **20**, 172–177 (2008).
6. D. C. Bellinger, A strategy for comparing the contributions of environmental chemicals and other risk factors to neurodevelopment of children. *Environ. Health Perspect.* **120**, 501–507 (2012).
7. J. Montgomery, J. Evans, S. Chenery, V. Pashley, K. Killgrove, "Gleaming, white and deadly": Using lead to track human exposure and geographic origins in the Roman period in Britain. *J. Roman Archaeol.* **78**, 199–226 (2010).
8. S. E. Schober, L. B. Mirel, B. I. Graubard, D. J. Brody, K. M. Flegal, Blood lead levels and death from all causes, cardiovascular disease, and cancer: Results from the NHANES III mortality study. *Environ. Health Perspect.* **114**, 1538–1541 (2006).
9. S. Lee, J.-Y. Min, K.-B. Min, Female infertility associated with blood lead and cadmium levels. *Int. J. Environ. Res. Public Health* **17**, 1794 (2020).
10. B. Lanphear *et al.*, Low-level environmental lead exposure and children's intellectual function: An international pooled analysis. *Environ. Health Perspect.* **113**, 894–899 (2005).
11. B. Lanphear *et al.*, Erratum: Low-level environmental lead exposure and children's intellectual function: An international pooled analysis. *Environ. Health Perspect.* **127**, 099001 (2019).
12. D. C. Bellinger, A. Malin, R. O. Wright, "Chapter one–The neurodevelopmental toxicity of lead: History, epidemiology, and public health implications" in *Advances in Neurotoxicology*, M. Aschner, L. G. Costa, Eds. (Academic Press, 2018), vol. 2, pp. 1–26.
13. J. Boyle, D. Yeter, M. Aschner, D. C. Wheeler, Estimated IQ points and lifetime earnings lost to early childhood blood lead levels in the United States. *Sci. Total Environ.* **778**, 146307 (2021).
14. J. Nriagu, The rise and fall of leaded gasoline. *Sci. Total Environ.* **92**, 13–28 (1990).
15. J. R. McConnell *et al.*, Hemispheric-scale heavy metal pollution from South American and Australian mining and metallurgy during the Common Era. *Sci. Total Environ.* **912**, 169431 (2024).
16. J. McConnell *et al.*, Lead pollution recorded in Greenland ice indicates European emissions tracked plagues, wars, and imperial expansion during antiquity. *Proc. Natl. Acad. Sci. U.S.A.* **115**, 5726–5731 (2018).
17. J. R. McConnell *et al.*, Pervasive Arctic lead pollution suggests substantial growth in medieval silver production modulated by plague, climate, and conflict. *Proc. Natl. Acad. Sci. U.S.A.* **116**, 14910–14915 (2019).
18. K. Rosman, W. Chisholm, S. Hong, J. Candelone, C. Boutron, Lead from Carthaginian and Roman Spanish mines isotopically identified in Greenland ice dated from 600 BC to 300 AD. *Environ. Sci. Technol.* **31**, 3413–3416 (1997).
19. C. C. Patterson, H. Shirahata, J. E. Ericson, Lead in ancient human bones and its relevance to historical developments of social problems with lead. *Sci. Total Environ.* **61**, 167–200 (1987).
20. L. Makra, "Chapter 18–Anthropogenic air pollution in ancient times" in *Toxicology in Antiquity*, P. Wexler, Ed. (Academic Press, ed. 2, 2019), pp. 267–287. 10.1016/B978-0-12-815339-0.00018-4.
21. T. Murphy, *Pliny the Elder's Natural History: The Empire in the Encyclopedia* (Oxford University Press, 2004).
22. S. R. Scott *et al.*, Applying trace element geochemistry of archaeological bone to study the coevolution of environmental change and human health in the Roman Empire. *Environ. Res.* **262**, 119941 (2024).
23. J. Moore *et al.*, Death metal: Evidence for the impact of lead poisoning on childhood health within the Roman Empire. *Int. J. Osteoarchaeol.* **31**, 846–856 (2021).
24. R. Bindler, Mired in the past–looking to the future: Geochemistry of peat and the analysis of past environmental changes. *Glob. Planet. Change* **53**, 2009–2221 (2006).
25. W. Shotyk *et al.*, History of atmospheric lead deposition since 12,370 C-14 yr BP from a peat bog, Jura Mountains, Switzerland. *Science* **281**, 1635–1640 (1998).
26. M. E. Kylander *et al.*, Refining the pre-industrial atmospheric Pb isotope evolution curve in Europe using an 8000 year old peat core from NW Spain. *Earth Planet. Sci. Lett.* **240**, 467–485 (2005).
27. S. M. Wensman, A. E. Shiel, J. R. McConnell, Lead isotopic fingerprinting of 250-years of industrial era pollution in Greenland ice. *Anthropocene* **38**, 100340 (2022).
28. A. Eichler *et al.*, Consistent histories of anthropogenic western European air pollution preserved in different Alpine ice cores. *Cryosphere* **17**, 2119–2137 (2023).
29. K. Butcher, M. Ponting, *The Metallurgy of Roman Silver Coinage: From the Reform of Nero to the Reform of Trajan* (Cambridge University Press, Cambridge, 2015).
30. J. M. Pacyna, E. G. Pacyna, An assessment of global and regional emissions of trace metals to the atmosphere from anthropogenic sources worldwide. *Environ. Rev.* **9**, 269–298 (2011).
31. A. Wilson, H. Friedman, Mining Database. Version 1.0, http://oxrep.classics.ox.ac.uk/databases/mines_database/.
32. J. O. Nriagu, "Lead and lead poisoning in antiquity" in *Environ. Sci. Technol.* (Wiley, 1983).
33. J. O. Nriagu, Occupational exposure to lead in ancient times. *Sci. Total Environ.* **31**, 105–116 (1983).
34. J. Scarborough, The myth of lead poisoning among the Romans: An essay review. *J. Hist. Med. Allied Sci.* **39**, 469–475 (1984).
35. C. C. Patterson, Silver stocks and losses in ancient and medieval times. *Econ. Hist. Rev.* **25**, 205–233 (1972).
36. S. M. Hong, J. P. Candelone, C. C. Patterson, C. F. Boutron, Greenland ice evidence of hemispheric lead pollution 2-millennia ago by Greek and Roman civilizations. *Science* **265**, 1841–1843 (1994).
37. L. Bakels *et al.*, FLEXPART version 11: Improved accuracy, efficiency, and flexibility. *EGUsphere* **2024**, 1–50 (2024).
38. S. Eckhardt *et al.*, Source-receptor matrix calculation for deposited mass with the Lagrangian particle dispersion model FLEXPART v10.2 in backward mode. *Geosci. Model Dev.* **10**, 4605–4618 (2017).
39. J. R. McConnell *et al.*, Hemispheric black carbon increase after the 13th-century Māori arrival in New Zealand. *Nature* **598**, 82–85 (2021).
40. P. Laloyaux, E. de Boisseson, P. Dahlgren, CERA-20C: An Earth system approach to climate reanalysis. *ECMWF Newsl.* **150**, 25–30 (2017).
41. S. R. Grobler, F. S. Theunissen, T. J. Kotze, The relation between lead concentrations in human dental tissues and in blood. *Arch. Oral Biol.* **45**, 607–609 (2000).
42. K. S. Crump, C. Van Landingham, T. S. Bowers, D. Cahoy, J. K. Chandalia, A statistical reevaluation of the data used in the Lanphear et al. (2005) pooled-analysis that related low levels of blood lead to intellectual deficits in children. *Crit. Rev. Toxicol.* **43**, 785–799 (2013).
43. K. B. Egan, C. R. Cornwell, J. G. Courtney, A. S. Ettinger, Blood lead levels in U.S. children ages 1–11 years, 1976–2016. *Environ. Health Perspect.* **129**, 037003 (2021).
44. M. Sullivan, *Tainted Earth: Smelters, Public Heath, and the Environment, Critical Issues in Health and Medicine* (Rutgers University Press, 2014).
45. J. E. Maskall, I. Thornton, Chemical partitioning of heavy metals in soils, clays and rocks at historical lead smelting sites. *Water Air Soil Pollut.* **108**, 391–409 (1998).
46. C. Fenga, S. Gangemi, V. Di Salvatore, L. Falzone, M. Libra, Immunological effects of occupational exposure to lead (Review). *Mol. Med. Rep.* **15**, 3355–3360 (2017).
47. K. Harper, *The Fate of Rome: Climate, Disease, and the End of an Empire, The Princeton History of the Ancient World* (Princeton University Press, Princeton, 2017).
48. J. R. McConnell *et al.*, Synchronous volcanic eruptions and abrupt climate change ~17.7 ka plausibly linked by stratospheric ozone depletion. *Proc. Natl. Acad. Sci. U.S.A.* **114**, 10035–10040 (2017).
49. J. R. McConnell, G. W. Lamorey, S. W. Lambert, K. C. Taylor, Continuous ice-core chemical analyses using inductively coupled plasma mass spectrometry. *Environ. Sci. Technol.* **36**, 7–11 (2002).
50. T. Opel, D. Fritzsche, H. Meyer, Eurasian Arctic climate over the past millennium as recorded in the Akademii Nauk ice core (Severnaya Zemlya). *Clim. Past* **9**, 2379–2389 (2013).
51. M. Simonsen *et al.*, East Greenland ice core dust record reveals timing of Greenland ice sheet advance and retreat. *Nat. Commun.* **10**, 4494 (2019).
52. M. M. Arienzo, J. R. McConnell, N. J. Chellman, S. Kipfstuhl, Method for correcting continuous ice-core elemental measurements for under-recovery. *Environ. Sci. Technol.* **53**, 5887–5894 (2019), 10.1021/acs.est.9b00199.
53. J. R. McConnell, A. J. Aristarain, J. R. Banta, P. R. Edwards, J. C. Simoes, 20th-century doubling in dust archived in an Antarctic Peninsula ice core parallels climate change and desertification in South America. *Proc. Natl. Acad. Sci. U.S.A.* **104**, 5743–5748 (2007).
54. H. Bowen, *Environmental Chemistry of the Elements* (Academic Press, London, 1979).
55. G. Sinnl *et al.*, A multi-ice-core, annual-layer-counted Greenland ice-core chronology for the last 3800 years: GICC21. *Clim. Past* **18**, 1125–1150 (2022).
56. M. Sigl *et al.*, Timing and climate forcing of volcanic eruptions for the past 2,500 years. *Nature* **523**, 543–549 (2015).
57. F. Adolphi, R. Muscheler, Synchronizing the Greenland ice core and radiocarbon timescales over the Holocene–Bayesian wiggle-matching of cosmogenic radionuclide records. *Clim. Past* **12**, 15–30 (2016).
58. J. R. McConnell *et al.*, Extreme climate after massive eruption of Alaska's Okmok volcano in 43 BCE and effects on the late Roman Republic and Ptolemaic Kingdom. *Proc. Natl. Acad. Sci. U.S.A.* **117**, 15443–15449 (2020).
59. A. Stohl, C. Forster, A. Frank, P. Seibert, G. Wotawa, Technical note: The Lagrangian particle dispersion model FLEXPART version 6.2. *Atmos. Chem. Phys.* **5**, 2461–2474 (2005).
60. H. Hersbach *et al.*, The ERA5 global reanalysis. *Q. J. R. Meteorol. Soc.* **146**, 1999–2049 (2020).
61. D. Weis *et al.*, High-precision isotopic characterization of USGS reference materials by TIMS and MC-ICP-MS. *Geochem. Geophys. Geosyst.* **7**, Q08006 (2006).
62. F. Velasco *et al.*, Geology and geochemistry of the Reocin zinc-lead deposit, Basque-Cantabrian Basin, Northern Spain. *Econ. Geol.* **98**, 1371–1396 (2003).
63. C. Pomiès, A. Cocherie, C. Guerrot, E. Marcoux, J. Lancelot, Assessment of the precision and accuracy of lead-isotope ratios measured by TIMS for geochemical applications: Example of massive sulphide deposits (Rio Tinto, Spain). *Chem. Geol.* **144**, 137–149 (1998).
64. F. Velasco, A. Pesquera, J. M. Herrero, Lead isotope study of Zn-Pb ore deposits associated with the Basque-Cantabrian basin and Paleozoic basement, Northern Spain. *Mineral. Deposita* **31**, 84–92 (1996).
65. L. Krahn, A. Baumann, Lead isotope systematics of epigenetic lead-zinc mineralization in the western part of the Rheinisches Schiefergebirge, Germany. *Mineral. Deposita* **31**, 225–237 (1996).
66. D. Large, R. Schaeffer, A. Höhndorf, Lead isotope data from selected galena occurrences in the North Eifel and North Sauerland, Germany. *Mineral. Deposita* **18**, 235–243 (1983).
67. Z. A. Stos-Gale *et al.*, Lead isotope data from the Isotrace Laboratory, Oxford: Archaeometry data base 5, ores from Bulgaria. *Archaeometry* **40**, 217–226 (1998).
68. R. Haggerty, P. Budd, B. Rohl, N. H. Gale, Pb-isotope evidence for the role of Mesozoic basins in the genesis of Mississippi Valley-type mineralization in Somerset, UK. *J. Geol. Soc.* **153**, 673–676 (1996).
69. B. M. Rohl, Lead isotope data from the Isotrace Laboratory, Oxford: Archaeometry data base 2, galena from Britain and Ireland. *Archaeometry* **38**, 165–180 (1996).
70. K. J. Westner, M. Vaxevanopoulos, J. Blichert-Toft, G. Davis, F. Albarède, Isotope and trace element compositions of silver-bearing ores in the Balkans as possible metal sources in antiquity. *J. Archaeol. Sci.* **155**, 105791 (2023).

71. S. Jankovic, The isotopic composition of lead in some Tertiary lead-zinc deposits within the Serbo-macedonian metallogenic province (Yugoslavia). *Ann. Geol. Pénins. Balk* **42**, 507–525 (1978).
72. Z. A. Stós-Gale, N. H. Gale, Sources of galena, lead and silver in Predynastic Egypt. *ArchéoSciences* **1**, 285–296 (1981).
73. Z. A. Stos-Gale, N. H. Gale, N. Annetts, Lead isotope data from the isotrace laboratory, Oxford: Archaeometry data base 3, ores from the Aegean, part 1. *Archaeometry* **38**, 381–390 (1996).
74. Z. A. Stos-Gale, N. H. Gale, OXALID: Oxford archaeological lead isotope database from the isotrace laboratory, https://oxalid.arch.ox.ac.uk/default.html.
75. M. Vaxevanopoulos, J. Blichert-Toft, G. Davis, F. Albarède, New findings of ancient Greek silver sources. *J. Archaeol. Sci.* **137**, 105474 (2022).
76. R. H. Brill, I. L. Barnes, W. R. Shields, T. J. Murphy, Isotopic analysis of Laurion lead ores. *Archaeol. Chem.* **138**, 1–10 (1974), 10.1021/ba-1974-0138.ch001.
77. S. Baron, C. G. Tămaş, B. Cauuet, M. Munoz, Lead isotope analyses of gold–silver ores from Roşia Montană (Romania): A first step of a metal provenance study of Roman mining activity in Alburnus Maior (Roman Dacia). *J. Archaeol. Sci.* **38**, 1090–1100 (2011).
78. R. Frei, "Isotope (Pb, Rb-Sr, S, O, C, U-Pb) geochemical investigations on Tertiary intrusives and related mineralizations in the Serbomacedonian Pb-Zn, Sb+ Cu-Mo metallogenetic province in northern Greece," PhD thesis, Swiss Federal Institute of Technology (ETH) (1992). 10.3929/ethz-a-000692261.
79. S. Baron, J. Carignan, S. Laurent, A. Ploquin, Medieval lead making on Mont-Lozère Massif (Cévennes-France): Tracing ore sources using Pb isotopes. *Appl. Geochem.* **21**, 241–252 (2006).
80. J. R. McConnell, R. Edwards, Coal burning leaves toxic heavy metal legacy in the Arctic. *Proc. Natl. Acad. Sci. U.S.A.* **105**, 12140–12144 (2008).